MIT Open Access Articles

Helical vortex formation in three-dimensional electrochemical systems with ion-selective membranes

Massachusetts Institute of Technology

Helical vortex formation in three-dimensional electrochemical systems with ion-selective membranes

Sang V. Pham,[1,2,3] Hyuckjin Kwon,[1,4] Bumjoo Kim,[1] Jacob K. White,[1] Geunbae Lim,[4] and Jongyoon Han[1,2,5,*]

[1]*Research Laboratory of Electronics, Department of Electrical Engineering and Computer Science, Massachusetts Institute of Technology, Cambridge, Massachusetts 02139, USA*

[2]*Singapore-MIT Alliance for Research and Technology (SMART), Singapore 138602*

[3]*Department of Ship Engineering and Fluid Mechanics, Hanoi University of Science and Technology, No1 DaiCoViet, Hanoi, Vietnam*

[4]*Pohang Universities of Science and Technology, Pohang, Gyeoungbuk 790784, Republic of Korea*

[5]*Department of Biological Engineering, Massachusetts Institute of Technology, Cambridge, Massachusetts 02139, USA*

The rate of electric-field-driven transport across ion-selective membranes can exceed the limit predicted by Nernst (the limiting current), and encouraging this "overlimiting" phenomenon can improve efficiency in many electrochemical systems. Overlimiting behavior is the result of electroconvectively induced vortex formation near membrane surfaces, a conclusion supported so far by two-dimensional (2D) theory and numerical simulation, as well as experiments. In this paper we show that the third dimension plays a critical role in overlimiting behavior. In particular, the vortex pattern in shear flow through wider channels is *helical* rather than planar, a surprising result first observed in three-dimensional (3D) simulation and then verified experimentally. We present a complete experimental and numerical characterization of a device exhibiting this recently discovered 3D electrokinetic instability, and show that the number of parallel helical vortices is a jump-discontinuous function of width, as is the overlimiting current and overlimiting conductance. In addition, we show that overlimiting occurs at lower fields in wider channels, because the associated helical vortices are more readily triggered than the planar vortices associated with narrow channels (effective 2D systems). These unexpected width dependencies arise in realistic electrochemical desalination systems, and have important ramifications for design optimization.

I. INTRODUCTION

Ion-exchange membranes are key elements of many electrochemical systems, including those used for desalination [1] and energy production (e.g., batteries and fuel cells) [2]. A curious and important characteristic of the current-voltage (*I-V*) relation in ion-exchange membranes is the presence of overlimiting current; at sufficiently high bias voltages, the rate of cross-membrane transport can exceed the so-called limiting current, posed by considering only diffusion and drift of ions. Several mechanisms have been suggested as the cause for overlimiting including water dissociation [1], gravitational convection [3–5], and electroconvection [6–9].

However, the preponderance of the recent theoretical, numerical, and experimental evidence now strongly favors electroconvection as the major mechanism behind overlimiting current. Electroconvection near ion-exchange membrane surfaces was first studied by Dukhin [6]. Later, Rubinstein and Zaltzman developed an electroconvection theory by assuming nonequilibrium electro-osmotic slip on ion-exchange membrane surfaces. They showed that allowing slip leads to instability in the concentration polarization at the membrane surface, an instability that causes a collapse of the diffusion layer, thereby enhancing overlimiting conductance [7–9]. This theoretical prediction was first validated indirectly in an experiment reported by Rubinstein *et al.* [10]. The presence of strong vortical flow in the overlimiting regime was observed directly in experiment [11–13]. In these experimental and theoretical studies, the instability is examined in quiescent solution, and is characterized by strong vortices forming in pairs. Kwak *et al.* [14] investigated the overlimiting regime for

the case of sheer flow, and reported a unidirectional vortex that develops in the overlimiting regime. Their shear flow example is especially relevant for applications such as electrodialysis (ED) and electrochemical separation.

The overlimiting behavior in systems with ion-selective membranes is a complicated multiscale multiphysics problem, so it is understandable that more work needs to be done on the two-dimensional case. Every aspect of the problem is more complicated in three dimensions: generalizing the analytical techniques is not straightforward; experimentally observing system behavior in the third dimension is technologically challenging; and extending recently developed 2D numerical simulation [15,16] to 3D proved to be computationally challenging [16]. Regardless, three-dimensional effects are far from inconsequential. In the overlimiting regime, wider channels sustain parallel *helical* vortices, a surprising result first observed in 3D simulation and then verified experimentally. The 3D simulation was performed using our customized Poisson-Nernst-Planck-Navier-Stokes solver, and the initial experiments were performed using our microscale electrical desalination system designed specifically for observing ion transport processes in detail [17]. Below we describe a comprehensive experimental and numerical characterization of a device exhibiting this recently discovered 3D electrokinetic instability. We give experimental and simulation evidence of helical vortex formation and show that the number of parallel helical vortices is a jump-discontinuous function of channel width, as is the overlimiting current and overlimiting conductance. In addition, we show that overlimiting occurs at lower fields in wider channels, probably because helical vortices are more readily triggered than the planar vortices associated with narrow channels. Finally, we show that helical vortices curiously merge in longer channels.
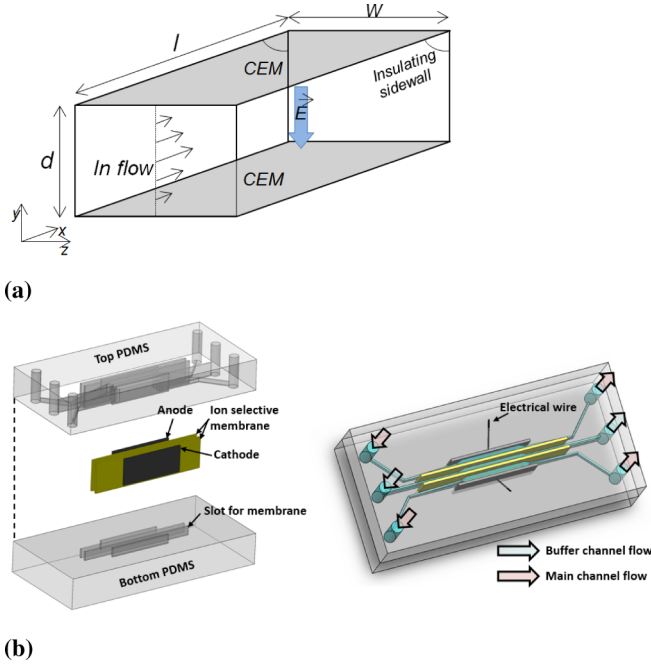
*jyhan@mit.edu

(a)

(b)

FIG. 1. (a) Schematic of ICP-desalination system including a microchannel with two CEMs located on top and bottom, and insulating sidewalls; electric field is introduced between the CEMs. (b) Design of ICP-desalination device used in the experiment.

II. PROBLEM MODEL

We consider a model system of an ion concentration polarization (ICP)–desalination device sketched in Fig. 1(a). The system includes a microchannel with cation-exchange membranes (CEMs) located on top and bottom. The microchannel has width w and depth d, with cation-exchange membranes at $y = 0$ and $y = d$, and insulating walls at $z = 0$ and $z = w$. Under electric field introduced between the CEMs, the near bottom CEMs region of salt solution flow is highly depleted, resulting in desalination effect in the lower half of the flow. Electric current is driven through the membrane by a bias voltage between the membranes. For experimental studying of 3D electrokinetic instability, we utilized a polydimethylsiloxane (PDMS)–based microfluidic device inserting cation-exchange membranes (CEMs) and a carbon electrode [Fig. 1(b)]. Fumasep FTCM-E (FuMA-Tech GmbH, Germany) and carbon paper (TGP-H-120, Toray) are used as CEM and electrode, respectively. To control the flow rate of main and buffer streams, a syringe pump (PHD2200, Harvard Apparatus) was used. A 1-mM sodium chloride (NaCl) solution is pumped at 15 mm/min into the main channel. For measuring the I-V response, applied voltage was swept from 0 to 20 V at 0.2 V/10 s. For visualizing the ion concentration polarization (ICP) phenomenon, Alexa Fluor 488 (Invitrogen, Carlsbad, CA) was added to the solution. A 3D image was captured with a Zeiss LSM 700 inverted laser scanning confocal microscope (1.58 μs/pixel scanning speed and 10-μm slice thickness) and processed using ZEN software. It should be noted that qualitatively similar behavior could also be observed in systems with either just anion-exchange membranes (AEMs), or with one CEM and one AEM (e.g., a

typical electrodialysis (ED) system), and the resulting physical interpretations will be similar to the ones presented below.

III. MATHEMATICAL MODEL AND NUMERICAL METHOD

In the ICP-desalination system, transport of ions is governed by the Nernst-Planck equations (1) and (2); electric potential field is related to the ion concentrations via the Poisson equations (3) and (4), and the fluid motion is governed by the Navier-Stokes equations (5) and (6). These equations are given in the dimensionless form as follows:

$$\frac{1}{\tilde{\lambda}_D} \frac{\partial \tilde{C}_{\pm}}{\partial \tilde{t}} = -\tilde{\nabla} \cdot \tilde{\mathbf{J}}_{\pm}, \tag{1}$$

$$\tilde{\mathbf{J}}_{\pm} = -\tilde{D}_{\pm}(\tilde{\nabla}\tilde{C}_{\pm} + Z_{\pm}\tilde{\nabla}\tilde{\Phi}) + \text{Pe}\,\tilde{\mathbf{U}}\tilde{C}_{\pm}, \tag{2}$$

$$\varepsilon^2 \tilde{\nabla}^2 \tilde{\Phi} = -\tilde{\rho}_e, \tag{3}$$

$$\tilde{\rho}_e = Z_+ \tilde{C}_+ + Z_- \tilde{C}_-, \tag{4}$$

$$\frac{1}{\text{Sc}} \frac{1}{\tilde{\lambda}_D} \frac{\partial \tilde{\mathbf{U}}}{\partial \tilde{t}} = -\tilde{\nabla}\tilde{P} + \tilde{\nabla}^2 \tilde{\mathbf{U}} - \text{Re}(\tilde{\mathbf{U}} \cdot \tilde{\nabla})\tilde{\mathbf{U}} - \frac{1}{\varepsilon^2}\tilde{\rho}_e \tilde{\nabla}\tilde{\Phi}, \tag{5}$$

$$\tilde{\nabla} \cdot \tilde{\mathbf{U}} = 0, \tag{6}$$

where $\tilde{t}, \tilde{C}_{\pm}, \tilde{\Phi}, \tilde{\mathbf{U}}, \tilde{P}$ denote the dimensionless time, ion concentration of cations (+) and anion (−), electric potential, vector of fluid velocity, and pressure, respectively. These quantities have been normalized by the following reference values for time, ionic concentration, electric potential, velocity, and pressure, respectively:

$$\begin{aligned} \tau_0 &= \frac{l_0^2}{D_0}, \quad C_0 = C_{\text{Bulk}}, \quad \Phi_0 = \frac{k_B T}{Ze}, \\ U_0 &= \frac{\epsilon \Phi_0}{\eta l_0}, \quad U_0 = \frac{\eta \mathrm{U}_0}{l_0}, \end{aligned} \tag{7}$$

where C_{Bulk} is the concentration of ions at the bulk space, l_0 is the characteristic length scale, $D_0 = 0.5(D_+ + D_-)$ is average diffusivity, k_B is the Boltzmann constant, T is the absolute temperature, e is the elementary charge, $Z = |Z_{\pm}|$ is ion valence, η is dynamics viscosity of solution, and ϵ is permittivity of the solvent. Parameters $\tilde{D}_{\pm} = D_{\pm}/D_0, \tilde{\lambda}_D = \lambda_D/l_0$, and $\tilde{\rho}_e = \rho_e/C_{\text{Bulk}}$ are nondimensional expressions of diffusion coefficients, the Debye length ($\lambda_D = \sqrt{\epsilon k_B T/2C_{\text{Bulk}} Z^2 e^2}$), and the space charge, respectively. $\text{Pe} = U_0 l_0/D_0$, $\text{Sc} = \eta/\rho_m D_0$, and $\text{Re} = U_0 l_0 \rho_m/\eta$, are the Péclet number, the Schmidt number, and the Reynolds number, respectively.

The system is characterized by the dimensionless Debye length $\tilde{\lambda}_D$. In this study, $\tilde{\lambda}_D = 0.001$, corresponds to the characteristic length $l_0 = 10\,\mu$m, bulk concentration $C_0 = 1\,\text{m}M(\text{NaCl})$, and absolute temperature $T = 300$ K. Other parameters used in the simulation include the diffusivities $D_+ = 1.33 \times 10^{-9}\,\text{m}^2\,\text{s}^{-1}$ and $D_- = 2.03 \times 10^{-9}\,\text{m}^2\,\text{s}^{-1}$.

For closure of the governing equations, the follows boundary conditions were used. At the inlet ($x = 0$), ionic species are well mixed, $\tilde{C}_+ = \tilde{C}_- = 1$; the fluid flow velocity is given. At the membranes' surface, the no-flux condition is enforced to anions $\tilde{\mathbf{J}}_- \cdot \vec{\mathbf{n}}$; cations are assumed to be accumulated uniformly at a concentration of $\tilde{C}_m$, ($\tilde{C}_+ = \tilde{C}_m = 2$) which is double the bulk concentration; the common no-slip boundary condition is enforced to the fluid. Bias voltage is applied to the system through the fixed-value boundary condition for electric potential at the top CEM ($\tilde{\Phi} = V$) and the bottom CEM ($\tilde{\Phi} = 0$).

Our device was modeled by numerically solving the Poisson-Nernst-Planck-Navier-Stokes equations (without chemical reactions), as described in [14,16]. The boundary conditions for closing the system of governing equations include fixing the cation concentration on the membrane surface (as proposed by Rubinstein and Zaltzman [7,8]), enforcing zero flux though CEMs for anions, and imposing no-slip conditions on the insulating walls. In addition, it was assumed that there was no surface charge on insulating walls, thereby ignoring surface conduction. The resulting system of time-dependent partial differential equations was divided in two, the Poisson-Nernst-Planck equations and the Navier-Stokes equations. At each time step, the interaction between the two sets of equation was resolved iteratively. In each iteration, the Poisson-Nernst-Planck equations were solved simultaneously using a Newton method, and the Navier-Stokes equations were solved using a staggered grid. In order to limit excessive grid refinement near membrane surfaces, the equations were solved with a dimensionless Debye length, $\lambda = 10^{-3}$, far larger than a physically realistic value (i.e., $\sim 10^{-4}$). Other studies [6,7,15–18] employ similar dimensionless Debye length values, and as shown below, the simulation results are clearly qualitatively similar to the realistic phenomenon observed in the experiment.

IV. RESULTS AND DISCUSSION

A. Helical structure of instability vortex

In Fig. 2, we show simulated (SIM) and measured (EXP) ion concentrations at the outlet and on the symmetry plane of a system with aspect ratio $w/d = 1$. Note that there is a good match between simulation and experiment, and that the results lead to two conclusions: (1) In the Ohmic and limiting regimes, there is little concentration variation in the width (z) direction, indicating only minor 3D effects; (2) in the overliming regime, however, the concentration profile in the width direction exhibits characteristic features of electrokinetic instability (also known as "Rubinstein and Zaltzman" instability [7], often found in 2D quiescent solutions) [7,12,13,15,16]. In particular, there appear to be side-by-side vortex pairs spanning the channel cross section, as shown in Fig. 2(f), a clear departure from the 2D planar vortices spanning the channel length, as observed by Kwak *et al.* [14] in their (otherwise similar) narrow channel experiment ($w/d = 0.2$ in [14]).

In Fig. 3, we compare the flow line plots generated from simulating the overliming behavior in a narrow [$w/d = 0.1$, Fig. 3(a)] and a wide [$w/d = 1$, Fig. 3(b)] device. The plots make clear that for narrow devices, the instability vortices are
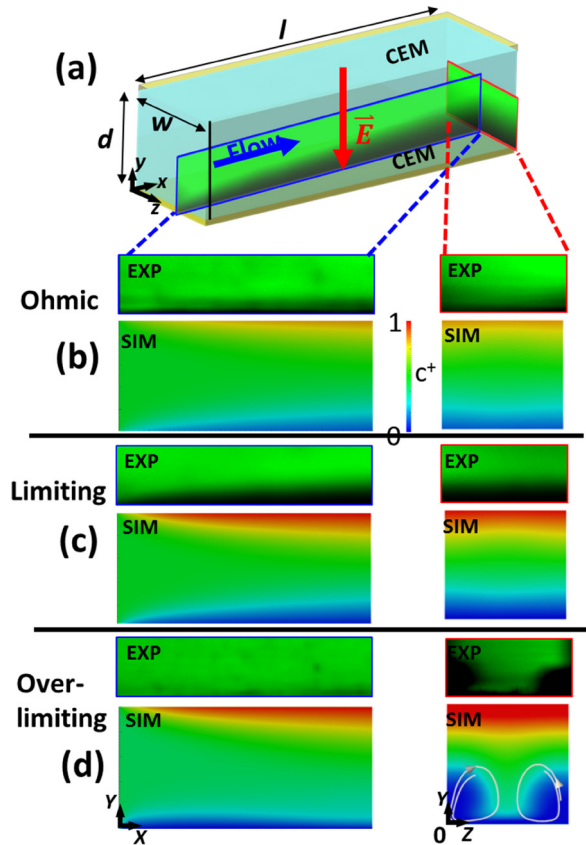

FIG. 2. Simulation result (SIM) and 3D microscopic image (EXP) for concentration at the outlet and on a symmetry plane are shown in different regimes: Ohmic (b), limiting (c), and overliming (d) for device with $w/d = 1$. Under electric field introduced between the CEMs, the near bottom CEMs region of salt solution is a highly depleted flow which is represented by blue in the simulation and by the dark region in the microscopic image. In Ohmic and limiting regimes, the ion depletion zone is uniform in the z direction and getting thicker as applied field increases (b,c) (note that a full cross-section picture is shown in SIM, while only the lower half is shown in EXP). In the overliming regime, helical vortices form at the corners resulting in a nonuniform depletion zone of which the thickness at midchannel is even thinner than in the limiting regime (c,d). Note that only in the lower half of the EXP cross section it is shown that the dimensions ($w/d/l$) of the experimental device and simulation model are $1/1/2$ mm and $10/10/25$ μm, respectively.

planar, and form circles that line up along the flow direction in a similar pattern to those observed in quiescent solution [11–13], or those observed in narrow channel shear flow [14]. In the wider device, however, the flow is remarkably different. As shown in Fig. 3(b), the electroconvective instability manifests itself as "corkscrew" or helical vortices. We verified, using both simulation and experiments, that when the width of the channel is above a critical aspect ratio ($w/d > 0.2$ in simulation and $w/d > 0.1$ in experiments), vortices form that are characterized by their helical structure, as shown in Fig. 3(b). This 3D instability can only be properly monitored by 3D microscopy. In addition, given the typical channel geometries used in electrodialysis and other systems, it is likely
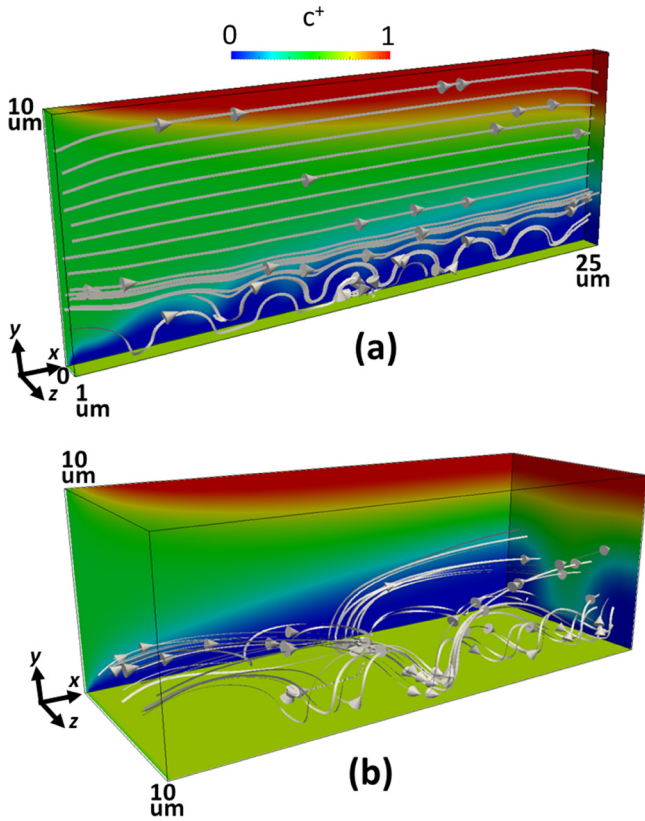
FIG. 3. Modeling observations for forms of instability vortex in narrow channel and wide channel. (a) Unidirectional vortices in channel with aspect ratio $w/d = 0.1/1$. (b) Helical vortex pair forming in channel with aspect ratio $w/d = 1/1$.

that this helical vortex pattern is prevalent in actual electrical desalination systems such as electrodialysis.

B. Impact of device width on overlimiting conductivity

The transition to helical vortex pairs, and in wider devices, to multiple pairs of helical vortices, has a conspicuous impact on device conductivity. As can be seen in Fig. 4(c), the measured overlimiting conductivity generally decreases with increasing width, but is punctuated with abrupt upward jumps. This trend can be explained by examining the schematic in Fig. 4(d), where ①, ② and ③ denote channels with increasing widths. As the channel width increases, the vortices widen but do not increase in number. Given that the applied field is unchanged, the velocity of the wider vortices is lower, and they are a less effective aid to ion transport. In addition, vortex sizes largely determine the depletion zone thickness, and wider vortices means thicker depletion zone with reduced conductivity. The result is a gradual decrease in conductivity, and is represented by the transition from ① to ② in Fig. 4(d). As the device is widened, the vortices will exceed a critical size and then break up and form additional faster, yet thinner, vortices. The jump in the number of vortices produces an upward jump in conductivity, and is represented by the transition from ② to ③, in Fig. 4(d). The measured conductivity jumps at $w/d = 0.7, 1.1$, and 1.7 in Fig. 4(c), roughly

corresponding to an increase in the number of accommodated vortex pairs in the channel.

As was verified by earlier experiments [11–13,14], over-limiting current though a permselective surface is associated with electroconvection instability, and its onset was shown to be controlled by membrane heterogeneity [7,9,19] and channel depth [20,21]. In this study, we are reporting that the initiation of overlimiting behavior from a realistic (3D) electrical desalination system is categorically different from the previously reported 2D behavior, mainly due to different instability (2D vs 3D) patterns. Figures 4(a) and 4(b) show simulated and experimental voltage-current responses for various channel width values. Note two features of the plots: (1) earlier onset of overlimiting current and (2) higher overlimiting slope, depending on the w/d value of the system. Results from both simulation and experiment suggest that overlimiting occurs at lower fields in wider devices because the trigger for helical vortex formation is the always-present nonuniform velocity field at membrane-sidewall junctions (created by no-slip walls). In addition, shear flow suppresses instability in the flow (x) direction, and inhibits the formation of the planar vortices associated with overlimiting in narrow channels.

C. Emergence in flow direction of helical vortices

As a final observation, we note that the helical vortices merge in longer channels. Figure 5 shows simulated and measured concentrations on multiple cross sections along
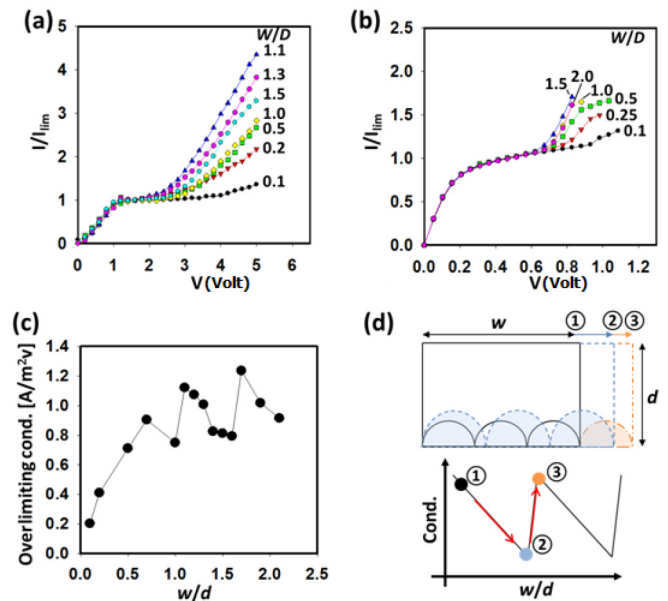

FIG. 4. *I-V* responses obtained in experiment (a) and simulation (b) for various w/d aspect ratios. (c) Measured conductance (representing slope in *I-V* response) in overlimiting regime for different aspect, showing jumps at $w/d = 0.7, 1.1$, and 1.7. (d) Simple diagram for explaining periodic characteristic in overlimiting conductance; ① → ② as channel width increases the vortices get thicker while the same number of vortex pairs remain, resulting in a decrease in overlimiting conductance; ② → ③ emergence of new vortex pairs leads a to a jump in the conductance.
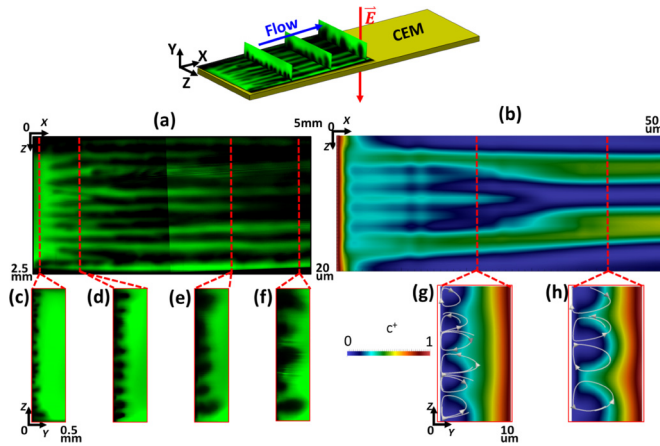
FIG. 5. Three-dimensional microscopic image (a,c–f) and simulation result (b,g,h) for concentration near bottom CEM. The helical vortex can be seen as dark long regions, indicating low concentration flow coming out from the depletion layer of the bottom CEM, merging down the stream, and leading to the change in number of depletion regions. Image of lateral cross section shows vortex merge indicated by depletion zone in both experiment ($w/d/l = 2.5/1/5$ mm) (a) and simulation ($w/d/l = 20/10/50$ μm) (b). (c–f) show depletion regions in the flow direction; merging process is exhibited though the change of number of vortices from 18 pairs at inlet to five pairs at outlet indicating merging of helical vortices. (g,h) corresponding picture from simulation. Note that in (c–f) only lower half of cross sections is shown.

the channel, and on a lateral cross section. In the earlier studies in quiescent solution, instability vortices develop in time from small seed vortices to pairs of big vortices, though a merging process [7,12,15,16]. However, the size selection criteria for the maximum vortex size was rather arbitrary (determined by the boundary condition); therefore it was not easy to employ the insight gained in a realistic membrane system. Here we reveal the spatial development of instability vortices, in a geometry that closely mimics the actual electrodialysis systems. We also propose a criterion by which 3D electroconvective instability is generated and maintained.

V. CONCLUSION

The newfound instability vortex structure, and the dependence of the vortex structure on 3D device parameters, is a more complete treatment of electrokinetic instability near ion-selective membranes, and will likely impact strategies for performance optimization of electrodialysis and other electrochemical devices.

[1] R. Simons, Desalination **28**, 41 (1979).

[2] T. V. Nguyen and R. E. White, J. Electrochem. Soc. **140**, 2178 (1993).

[3] M. Block and J. A. Kitchener, J. Electrochem. Soc. **113**, 947 (1966).

[4] S. Reich, B. Gavish, and S. Lifson, Desalination **24**, 295 (1977).

[5] Q. Li, Y. Fang, and M. E. Green, J Colloid Interface Sci. **91**, 412 (1983).

[6] S. S. Dukhin, Adv. Colloid Interface Sci. **35**, 173 (1991).

[7] I. Rubinstein and B. Zaltzman, Phys. Rev. E **62**, 2238 (2000).

[8] I. Rubinstein and B. Zaltzman, Math. Models Methods Appl. Sci. **11**, 263 (2001).

[9] T. Pundik, I. Rubinstein, and B. Zaltzman, Phys. Rev. E **72**, 061502 (2005).

[10] I. Rubinshtein, B. Zaltzman, J. Pretz, and C. Linder, Russ J. Electrochem. **38**, 853 (2002).

[11] S. J. Kim, Y.-C. Wang, J. H. Lee, H. Jang, and J. Han, Phys. Rev. Lett. **99**, 044501 (2007).

[12] G. Yossifon and H.-C. Chang, Phys. Rev. Lett. **101**, 254501 (2008).

[13] S. M. Rubinstein, G. Manukyan, A. Staicu, I. Rubinstein, B. Zaltzman, R. G. H. Lammertink, F. Mugele, and M. Wessling, Phys. Rev. Lett. **101**, 236101 (2008).

[14] R. Kwak, V. S. Pham, K. M. Lim, and J. Han, Phys. Rev. Lett. **110**, 114501 (2013).

[15] E. A. Demekhin, V. S. Shelistov, and S. V. Polyanskikh, Phys. Rev. E **84**, 036318 (2011).

[16] V. S. Pham, Z. Li, K. M. Lim, J. K. White, and J. Han, Phys Rev. E **86**, 046310 (2012).

[17] E. V. Dydek, B. Zaltzman, I. Rubinstein, D. S. Deng, A. Mani, and M. Z. Bazant, Phys. Rev. Lett. **107**, 118301 (2011).

[18] E. A. Demekhin, N. V. Nikitin, and V. S. Shelistov, Phys. Rev. E **90**, 013031 (2014).

[19] J. Balster, M. H. Yildirim, D. F. Stamatialis, R. Ibanez, R. G. H. Lammertink, V. Jordan, and M. Wessling, J Phys. Chem. B **111**, 2152 (2007).

[20] G. Yossifon, P. Mushenheim, and H. C. Chang, Europhys. Lett. **90**, 64004 (2010).

[21] J. Schiffbauer, E. A. Demekhin, and G. Ganchenko, Phys. Rev. E **85**, 055302(R) (2012).